Publisher: NPG; Journal: Nature: Nature; Article Type: Physics letter
DOI: 10.1038/nature08880

Intense star formation within resolved compact regions in a galaxy at z = 2.3

A. M. Swinbank[1], I. Smail[1], S. Longmore[2], A. I. Harris[3], A. J. Baker[4], C. De Breuck[5], J. Richard[1], A. C. Edge[1], R. J. Ivison[6,7], R. Blundell[2], K. E. K. Coppin[1], P. Cox[8], M. Gurwell[2], L. J. Hainline[3], M. Krips[8], A. Lundgren[9], R. Neri[8], B. Siana[10], G. Siringo[9], D. Stark[11], D. Wilner[2] & J. D. Younger[12]

[1]Institute for Computational Cosmology, Durham University, South Road, Durham DH1 3LE, UK. [2]Harvard-Smithsonian Center For Astrophysics, 60 Garden Street, Cambridge, Massachusetts 02138, USA. [3]Department of Astronomy, University of Maryland, College Park, Maryland 20742, USA. [4]Department of Physics and Astronomy, Rutgers, University of New Jersey, 136 Frelinghuysen Road, Piscataway, New Jersey 08854-8019, USA. [5]European Southern Observatory, Karl-Schwarzschild Strasse, 85748 Garching bei München, Germany. [6]UK Astronomy Technology Centre, Science and Technology Facilities Council, Royal Observatory, Blackford Hill, Edinburgh EH9 3HJ, UK. [7]Institute for Astronomy, Royal Observatory of Edinburgh, Blackford Hill, Edinburgh EH9 3HJ, UK. [8]Institut de Radio Astronomie Millimétrique, 300 Rue de la Piscine, Domaine Universitaire, 38406 Saint Martin d'Héres, France. [9]European Southern Observatory, Alonso de Cordova 3107, Cassilla 19001, Santiago 19, Chile. [10]California Institute of Technology, MS 105-24, Pasadena, California 91125, USA. [11]Institute of Astronomy, University of Cambridge, Madingley Road, Cambridge CB3 0HA, USA. [12]Institute for Advanced Study, Einstein Drive, Princeton, New Jersey 08540, USA.

Massive galaxies in the early Universe have been shown to be forming stars at surprisingly high rates[1–3]. Prominent examples are dust-obscured galaxies which are luminous when observed at sub-millimetre wavelengths and which may be forming stars at a rate of 1,000 solar masses ($M_{\odot}$) per year[4–7]. These intense bursts of star formation are believed to be driven by mergers between gas-rich galaxies[8–9]. Probing the properties of individual star-forming regions within these galaxies, however, is beyond the spatial resolution and sensitivity of even the largest telescopes at present. Here we report observations of the sub-millimetre galaxy SMMJ2135−0102 at redshift z = 2.3259, which has been gravitationally magnified by a factor of 32 by a massive foreground galaxy cluster lens. This magnification, when combined with high-resolution sub-millimetre imaging, resolves the star-forming regions at a linear scale of only 100 parsecs. We find that the luminosity densities of these star-forming regions are comparable to the dense cores of giant molecular clouds in the local Universe, but they are about a hundred times larger and 10^7 times more luminous. Although vigorously star-forming, the underlying physics of the star-formation processes at $z \approx 2$ appears to be similar to that seen in local galaxies, although the energetics are unlike anything found in the present-day Universe.

Strong gravitational lensing—light bent by massive galaxy clusters—magnifies the images of distant galaxies that serendipitously lie behind them, offering us a direct way to probe the physical processes occurring within star-forming regions in high-redshift galaxies. During an 870-μm

Publisher: NPG; Journal: Nature: Nature; Article Type: Physics letter
DOI: 10.1038/nature08880

observation using the Large Apex Bolometer Camera (LABOCA) on the Atacama Pathfinder Experiment (APEX) telescope of the massive galaxy cluster MACSJ2135-010217 ($z_{cluster}$ = 0.325), we recently discovered a uniquely bright galaxy with an 870-μm flux of 106.0 ± 7.0 mJy (Fig. 1). The optical and near-infrared counterpart is faint, with magnitude I_{AB} = 23.6 ± 0.2 and K_{AB} = 19.77 ± 0.07, but is extended along a roughly east–west direction, consistent with it being a gravitationally lensed background galaxy. The mid- and far-infrared colours (S_{24}/S_{70} = 0.4 ± 0.2) and red optical/near-infrared colours also suggest that the galaxy lies beyond the cluster at z > 1.5 (ref. 10 and Supplementary Information), and indeed detection of carbon monoxide (CO) J = 1–0 emission at 34.64 GHz unambiguously identified the redshift as z = 2.3259 ± 0.0001 (Fig. 2). With source and lens redshifts known, we used the gravitational lens model of the galaxy cluster (Supplementary Information) to correct for the lensing distortion, deriving an amplification factor for the background galaxy of μ = 32.5 ± 4.5.

Observations of molecular and continuum emission provide gas and stellar mass estimates. The observed velocity-integrated flux in CO(1–0) is f_{CO} = 2.3 ± 0.1 Jy km s^{-1}, and the CO(3–2)/CO(1–0) flux ratio of 5.9 ± 0.3 suggest that the molecular gas is subthermally excited (Fig. 2). Assuming a CO–H_2 conversion factor of α = 0.8 (K km s^{-1} pc^{-2})$^{-1}$ (which is appropriate for the smoothly distributed, high-pressure, largely molecular, interstellar medium with subthermal CO excitation[9,11,12]) we derive a cold gas mass of $M_{gas} = M_{(H2 + He)} = \alpha L'_{CO(1–0)} = (1.6 \pm 0.1) \times 10^{10} M_{\odot}$. (where $L'_{CO(1–0)}$ is the CO(1-0) emission line luminosity**).** We estimate the stellar mass by fitting stellar population synthesis models to the rest-frame ultraviolet–near-infrared spectral energy distribution[13] shown in Fig. 3. The best-fit spectral energy distributions have a range of ages from 10–30 Myr with significant dust extinction, $E(B - V)$ = 1.0 ± 0.1, and a stellar mass (corrected for lensing) of $M_{star} = 3 \pm 1 \times 10^{10} M_{\odot}$. Taken together, these imply a baryonic mass of $M_{bary} = M_{gas} + M_{star} = (4 \pm 2) \times 10^{10} M_{\odot}$, with approximately 35% of this in cold molecular gas.

Rest-frame far-infrared radiation from dust-reprocessed ultraviolet light provides an extinction-free measure of the instantaneous star-formation rate of a galaxy. Correcting for lens magnification, the intrinsic observed-frame 870-μm flux is $S_{870\,\mu m}$ = (3.0 ± 0.4) mJy, suggestive of a typical high-redshift ultra-luminous infrared galaxy[1,3,14]. Observations at 350 μm with APEX/SABOCA and at 434 μm with the Sub-Millimeter Array constrain the far-infrared spectral energy distribution (Fig. 3). Using a modified blackbody spectrum[3] with a two-component dust model (with dust temperature T_d = 30 K and 60 K) we derive a bolometric luminosity (corrected for lensing amplification) of $L_{bol} = (1.2 \pm 0.2) \times 10^{12}$ solar luminosities ($L_{\odot}$), suggesting a star-formation

Publisher: NPG; Journal: Nature: Nature; Article Type: Physics letter
DOI: 10.1038/nature08880

rate of $(210 \pm 50)M_{\odot}$ per year (ref. 15). If this star-formation rate has been continuous, it would take just ~150 Myr to build the current stellar mass; the remaining gas depletion timescale would be a further 75 Myr, suggesting that the intense star-formation episode we observe may be the first major growth phase of this galaxy. To set the global properties of the galaxy in the context of other galaxy populations, it is also possible to calculate the efficiency with which the dense gas is converted into stars. The theoretical limit at which stars can form[16] is given by a star-formation rate of $\varepsilon M_{\rm gas}/t_{\rm dyn}$ where ε is the star-formation efficiency, and $t_{\rm dyn}$ is the dynamical (free-fall) time, given by $t_{\rm dyn} = (r^3/2GM_{gas})^{0.5}$. Adopting $r = 1.5$ kpc, the star-formation efficiency is $\varepsilon \approx 0.02$, which is consistent with that derived for local ultra-luminous infrared galaxies[17] and archetypal high-redshift sub-millimetre galaxies[9], but a factor of 20 lower than the most extreme 'hyper'-starbursts at $z \approx 6$ (ref. 18).

Sub-Millimeter Array observations spatially resolve the galaxy's 870-μm (345-GHz) continuum emission with a 0.2″ synthesized beam, providing a detailed view of the galaxy's morphology. Figure 1 shows eight discrete components over ~4″ in projection. These represent two mirror images of the source, each comprising four separate emission regions, reflected about the lensing critical curve. The map contains a total flux of $S_{850\,\mu\rm m} = (86 \pm 3)$ mJy, or (82 ± 2)% of the flux in the LABOCA map, suggesting that the structures in the Sub-Millimeter Array map contain the bulk of the 870-μm luminosity. Reconstructing the source-plane image, the galaxy comprises four bright star-forming regions in the source plane (A, B, C and D), which are separated by 1.5 kpc in projection (A and B are separated by ~800 pc, C and D by ~450 pc). Assuming the dynamics of the CO emission trace the virialized potential well of the galaxy, then on these scales the dynamical mass of the system is $M_{\rm dyn} \approx (4–8) \times 10^{10} M_{\odot}$, in good agreement with the gas and stellar mass estimates.

For the most highly amplified components (D1 and D2, Fig. 1), the source-plane resolution reaches ~90 parsecs, only slightly larger than the ~60-parsec characteristic size of giant molecular clouds in the Milky Way[19]. This is consistent with the black-body radius ($R_{\rm bb}$) estimated from the bolometric luminosity and dust temperature via the scaling relation $L_{\rm bol}/L_{\odot} = (R_{\rm bb}/R_{\odot})^2 (T_{\rm d}/T_{\odot})^4$, where $R_{\rm bb}$ is the physical black-body radius and $T_{\odot}$ denotes the solar temperature)[20]. Taking $L_{\rm bol} = (0.6–1.1) \times 10^{12} L_{\odot}$, and assuming characteristic dust temperatures of $T_{\rm d} = 30–60$ K for each of the star-forming regions within SMMJ2135−0102, the predicted sizes are $R_{\rm bb} \approx 100–300$ pc. This is consistent with those measured on the sky at 870 μm.

Given that the star-forming regions in SMMJ2135−0102 are similar in size to giant molecular clouds in the Milky Way and Local Group galaxies, it is instructive to see how their luminosities

compare. The constant energy density within typical star-forming regions produces a correlation between size and luminosity such that $L_{260} \propto r^3$, which appears to hold over a wide range of sizes from 1–100 pc (refs 19–23; Fig. 4). In the star-forming cores within giant molecular clouds, however, the high luminosities from massive stars produce luminosity densities about 100 times higher than compared to the average across the cloud[24]. We therefore plot two lines in Fig. 4 with slope 3 (meaning a constant energy density), one representing the mean luminosity density within giant molecular clouds and the other representing a luminosity density a factor of 100 higher. The star-forming regions within SMMJ2135−0102 are about 100 pc across, two orders of magnitude larger than the one parsec seen for dense giant-molecular-cloud cores locally, but as Fig. 4 shows, their luminosities are approximately 100 times higher than expected for typical star-forming regions of comparable size in the low-redshift Universe. This means that the variable is most probably the number of star-forming cores, such that a region in SMMJ2135-0102 that has a size of ~100 pc contains ~10^7 one-parsec-sized cores[24–26]. The luminosity (and therefore star-formation) density of the star-forming regions within SMMJ2135-0102 are also similar to those found in the highest-density regions of the local starburst galaxy Arp220, although they are scaled up by a factor of ten in both size and luminosity[27] (Supplementary Information). Thus, although the energetics of the star-forming regions within SMMJ2135-0102 are unlike anything found in the present-day Universe, the relation between their size and luminosity is similar to local, dense giant-molecular-cloud cores, suggesting that the underlying physics of the star-forming processes is similar. These results suggest that the recipes developed to understand star-forming processes in the Milky Way and local galaxies can be used to model the star-formation processes in these high-redshift galaxies.

Received 20 October 2009; accepted 1 February 2010; doi:10.1038/nature08880.

<jrn>1. Chapman, S. C. *et al.* A redshift survey of the submillimeter galaxy population. *Astrophys. J.* **622,** 772–796 (2005).</jrn>

<jrn>2. Genzel, R. *et al.* The rapid formation of a large rotating disk galaxy three billion years after the Big Bang. *Nature* **442,** 786–796 (2006).</jrn>

<jrn>3. Coppin, K. *et al.* The SCUBA Half Degree Extragalactic Survey—VI. 350-μm mapping of submillimetre galaxies. *Mon. Not. R. Astron. Soc.* **384,** 1597–1610 (2008).</jrn>

<jrn>4. Smail, I. *et al.* A deep sub-millimeter survey of lensing clusters: a new window on galaxy formation and evolution. *Astrophys. J.* **490,** 5–8 (1997).</jrn>

<jrn>5. Hughes, D. H. *et al.* High-redshift star formation in the Hubble Deep Field revealed by a submillimetre-wavelength survey. *Nature* **394,** 241–247 (1998).</jrn>

<unknown>6. Blain, A. W. *et al.* Submillimeter galaxies. *Physics Reports.* **369,** 111–176 (2002).</unknown>

<jrn>7. Lilly, S. J. *et al*. The Canada-United Kingdom deep submillimeter survey. II. First identifications, redshifts, and implications for galaxy evolution. *Astrophys. J.* **518,** 641–655 (1999).</jrn>

<jrn>8. Swinbank, A. M. *et al.* The link between submillimetre galaxies and luminous ellipticals: near-infrared IFU spectroscopy of submillimetre galaxies. *Mon. Not. R. Astron. Soc.* **371,** 465–476 (2006).</jrn>

<jrn>9. Tacconi, L. J. *et al.* Submillimeter galaxies at z ~ 2: evidence for major mergers and constraints on lifetimes, IMF, and CO-H_2 conversion factor. *Astrophys. J.* **680,** 246–262 (2008).</jrn>

<jrn>10. Yun, M. S. *et al.* Spitzer IRAC infrared colours of submillimetre-bright. *Mon. Not. R. Astron. Soc.* **389,** 333–340 (2008).</jrn>

<jrn>11. Greve, T. R. *et al.* An interferometric CO survey of luminous submillimetre galaxies. *Mon. Not. R. Astron. Soc.* **359,** 1165–1183 (2005).</jrn>

<jrn>12. Solomon, P. M. & Vanden Bout, P. A. **Molecular Gas at High Redshift.** *Annu. Rev. Astron. Astrophys.* **43,** 677–725 (2005).</jrn>

<jrn>13. Bruzual, G. & Charlot, S. Stellar population synthesis at the resolution of 2003. *Mon. Not. R. Astron. Soc.* **344,** 1000–1028 (2003).</jrn>

<jrn>14. Chapman, S. C. *et al.* A median redshift of 2.4 for galaxies bright at submillimetre wavelengths. *Nature* **422,** 695–698 (2003).</jrn>

<jrn>15. Kennicutt, R. Star formation in galaxies along the Hubble sequence. Annu. Rev. of *Astron. Astrophys.* **36,** 189–232 (1998).</jrn>

<jrn>16. Elmegreen, B. G. Galactic bulge formation as a maximum intensity starburst. *Astrophys. J.* **517,** 103–107 (1999).</jrn>

<jrn>17. Gao, Y. & Solomon, P. M. HCN survey of normal spiral, infrared-luminous, and ultraluminous galaxies. *Astrophys. J.* (Suppl.) **152,** 63–80 (2004).</jrn>

<jrn>18. Walter, F. *et al.* A kiloparsec-scale hyper-starburst in a quasar host less than 1 gigayear after the Big Bang. *Nature* **457,** 699–701 (2009).</jrn>

<jrn>19. Scoville, N. Z. *et al.* The far-infrared luminosity of molecular clouds in the Galaxy.

Astrophys. J. **339,** 149–162 (1989).</jrn>

<jrn>20. Downes, D. *et al.* New observations and a new interpretation of CO(3–2) in IRAS F10214+4724. *Astrophys. J.* **453,** L65–L68 (1995).</jrn>

<jrn>21. Snell, R. *et al.* Molecular clouds and infrared stellar clusters in the far outer galaxy. *Astrophys. J.* **578,** 229–244 (2002).</jrn>

<jrn>22. Caldwell, D. A. *et al.* Star formation activity in the Large Magellanic Cloud: far-infrared emission from IRAS high-resolution data. *Astrophys. J.* **472,** 611–623 (1996).</jrn>

<jrn>23. Livanou, E. *et al.* Star-burst regions in the LMC. *Astron. Astrophys.* **451,** 431–434 (2006).</jrn>

<jrn>24. Hill, T. *et al.* Millimetre continuum observations of southern massive star formation regions—I. SIMBA observations of cold cores. *Mon. Not. R. Astron. Soc.* **363,** 405–451 (2005).</jrn>

<jrn>25. Lintott, C. *et al.* Hot cores: probes of high-redshift galaxies? *Mon. Not. R. Astron. Soc.* **360,** 1527–1531 (2002).</jrn>

<jrn>26. Carilli, C. *et al.* High-resolution imaging of molecular line emission from high-redshift QSOs. *Astrophys. J.* **123,** 1838–1846 (2002).</jrn>

<jrn>27. Sakamoto, K. *et al.* Submillimeter array imaging of the CO(3–2) line and 860μm continuum of Arp 220: tracing the spatial distribution of luminosity. *Astrophys. J.* **684,** 957–977 (2008).</jrn>

<unknown>28. Harris, A. I. *et al.* The Zpectrometer: an ultra-wideband spectrometer for the green bank telescope. *Astronomical Society of the Pacific Conference Series***375,** 82–93 (2007).</unknown>

Supplementary Information is linked to the online version of the paper at www.nature.com/nature.

Acknowledgements We thank the staff at Green Bank Telescope for scheduling the Zpectrometer observations at short notice, and the ESO director for granting directors discretionary time observations with SABOCA. A.M.S. gratefully acknowledges a Royal Astronomical Society Sir Norman Lockyer Fellowship, and J.R. and D.P.S. acknowledge a Marie Curie fellowship and a Science Technology and Facilities Council fellowship respectively. J.D.Y. acknowledges support from NASA through a Hubble Fellowship. The Zpectrometer observations were carried out on the Robert C. Byrd Green Bank Telescope, which is operated by the National Radio Astronomy Observatory, a facility of the National Science Foundation operated under cooperative agreement by Associated Universities, Inc. The APEX observations were carried out with ESO Telescopes. The 870 μm interferometric observations were carried out with the Sub-Millimeter Array, which is a joint project between the Smithsonian Astrophysical Observatory and the Academia Sinica Institute of

Publisher: NPG; Journal: Nature: Nature; Article Type: Physics letter
DOI: 10.1038/nature08880

Astronomy and Astrophysics and is funded by the Smithsonian Institution and the Academia Sinica. The CO(3-2) observations were carried out with the Plateua de Bure Interferometer which is supported by INSU/CNRS (France), Max Planck Gesellschaft (MPG; Germany), and Instituto Geográfico Nacional (IGN; Spain). J. D. Y. is a Hubble Fellow.

Author Contributions A.M.S., I.S., R.J.I. and A.C.E. designed and proposed the observations, collected the data and performed the multi-wavelength analysis. A.I.H., A.J.B. and L.J.H. conducted the Green Bank Telescope/Zpectrometer observations and reduced and analysed the data. C.D.B, A.L. and G.S. carried out the LABOCA and SABOCA observations and wrote a data-reduction pipeline. B.S. proposed and reduced the mid-infrared *Spitzer* observations. K.E.K.C. carried out the far-infrared spectral energy distribution fitting. S.L., R.B., M.G., D.W. and J.D.Y. conducted the Sub-Millimeter Array observations and reduced the data. P.C., M.K. and R.N carried out the PdBI observations and reduced the data. J.R. constructed the gravitational lensing model. D.P.S. carried out the optical/near-infrared spectral energy distribution modelling. All co-authors discussed the results and commented on the manuscript.

Author Information Reprints and permissions information is available at www.nature.com/reprints. The authors declare no competing financial interests. Correspondence and requests for materials should be addressed to A.M.S. (a.m.swinbank@dur.ac.uk).

Publisher: NPG; Journal: Nature: Nature; Article Type: Physics letter
DOI: 10.1038/nature08880

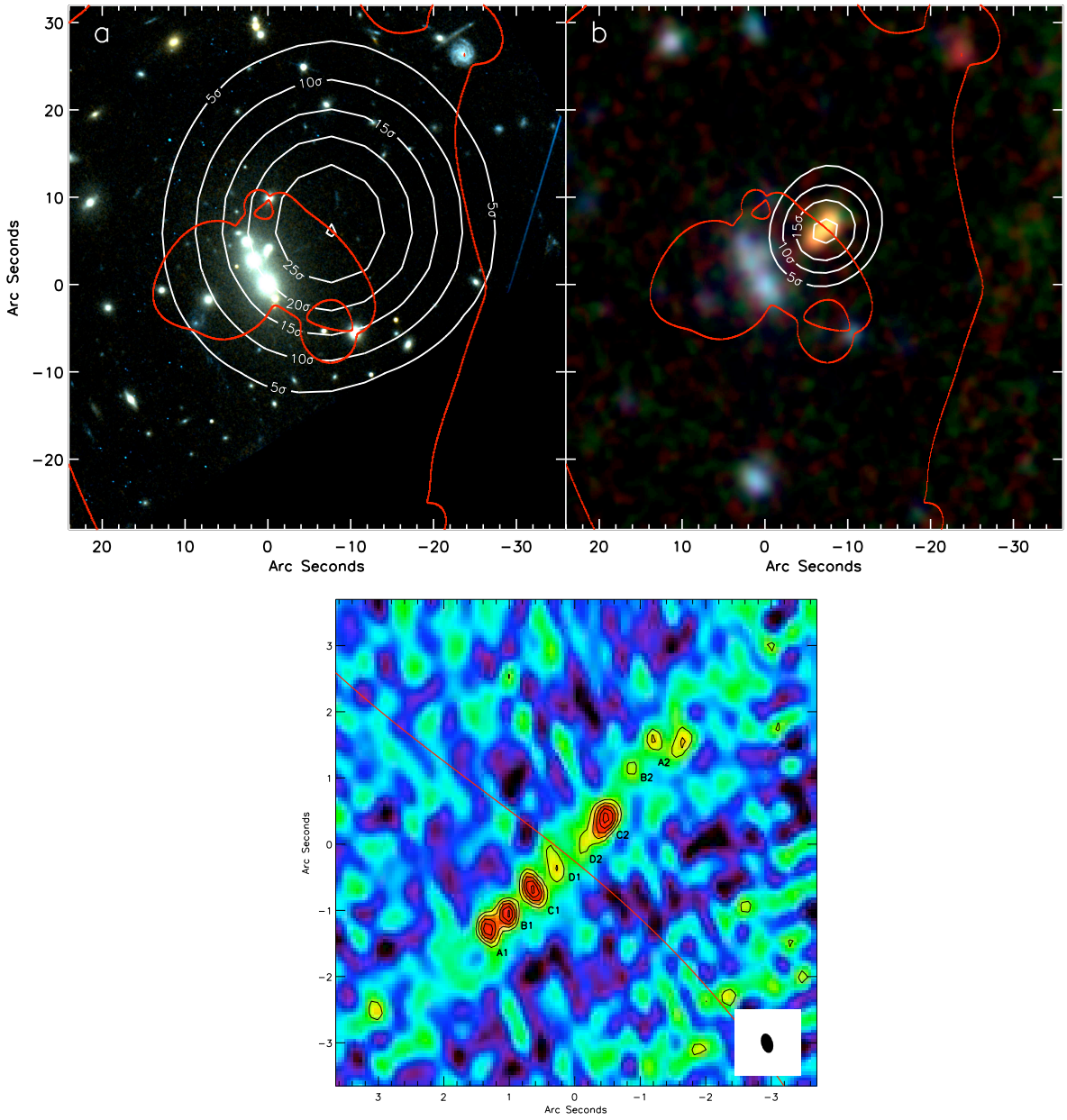

Figure 1 Multi-wavelength images of the galaxy cluster MACSJ2135-0102. a, Hubble Space Telescope VI-band colour image of the galaxy cluster with white contours denoting the 870-μm emission from observations with LABOCA on the APEX telescope. Contours denote 5σ, 10σ, 15σ, 20σ, 25σ and 30σ (with root-mean-square noise of 3.5 mJy), identifying a sub-millimetre galaxy with flux 106.0 ± 7.0 mJy (the quoted error on the galaxy flux includes calibration uncertainties) at α = 21:35:11.6, δ = –01:02:52.0 (J2000), which is associated with a faint optical counterpart with magnitude I_{AB} = 23.6 ± 0.2. The solid red lines denote the z = 2.326 radial and tangential critical curves from the best-fit lens model. **b**, True-colour IRAC 3.6 μm, 4.5 μm, 8.0 μm image of the

Publisher: NPG; Journal: Nature: Nature; Article Type: Physics letter
DOI: 10.1038/nature08880

cluster core with contours denoting the 350-μm emission from observations with the Submillimetre APEX Bolometer Camera (SABOCA). Contours are spaced at 5σ, 10σ, 15σ and 20σ (with root-mean-square noise of 23 mJy); the 350 μm flux is 530 ± 60 mJy. The mid-infrared counterpart is clearly visible as an extended red galaxy centred at the sub-millimetre position. The LABOCA and SABOCA full-width at half-maximum (FWHM) beams are 19″ and 8″ respectively. The origins of both images are on the lensed galaxy with north up and east left. **c**, Sub-Millimeter Array 870-μm image of the lensed galaxy. The map shows eight individual components, separated by up to 4″ in projection. The contours denote the 870μm emission and start at 3σ and are spaced by 1σ (where 1σ is 2.1mJy). The red line is the same $z = 2.326$ radial critical curve as in **a** and **b**. The components (A, B, C and D) represent two mirror images of the galaxy, each comprising four separate emission regions reflected about the lensing critical curve. The inset shows the 0.33″ × 0.21″ synthesized beam with position angle of 15° east of north.

Publisher: NPG; Journal: Nature: Nature; Article Type: Physics letter
DOI: 10.1038/nature08880

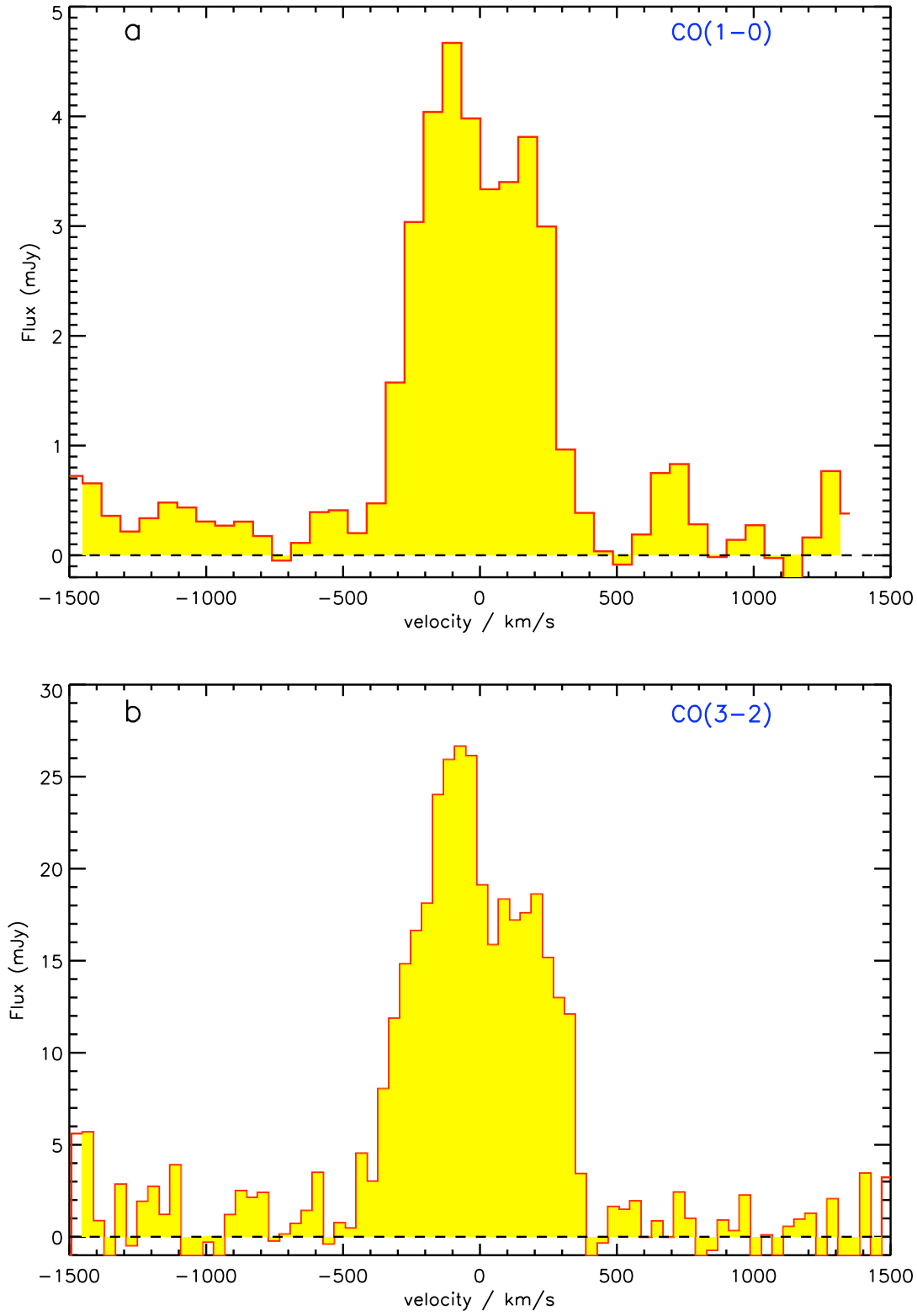

Figure 2 Carbon monoxide observations of SMMJ2135−0102 obtained with the Green Bank Telescope and Plateau de Bure Interferometer. The redshift of $z = 2.3259 \pm 0.0001$ was derived

Publisher: NPG; Journal: Nature: Nature; Article Type: Physics letter
DOI: 10.1038/nature08880

from observations using Zpectrometer, a wide-band spectral instrument on the Green Bank Telescope[28]. **a**, Zpectrometer CO(1–0) spectrum, showing a double-horned profile with a velocity offset of (290 ± 30) km s^{-1} between the two peaks. **b**, Plateau de Bure observations of the CO(3–2) emission, confirming both the redshift and the multiple velocity components seen in CO(1–0). The CO(3–2)/CO(1–0) flux ratio of 5.9 ± 0.3 suggests that the molecular gas is subthermally excited and we therefore derive a cold gas mass of $M_{\rm gas} = M_{\rm (H2+He)} = \alpha L'_{\rm CO(1-0)} = (1.6 \pm 0.1) \times 10^{10} M_{\odot}$ with $\alpha = 0.8$ (we adopt a cosmology with $\Omega_{\Lambda} = 0.73$, $\Omega_{\rm m} = 0.27$ and $H_0 = 72$ km s^{-1} Mpc^{-1}).

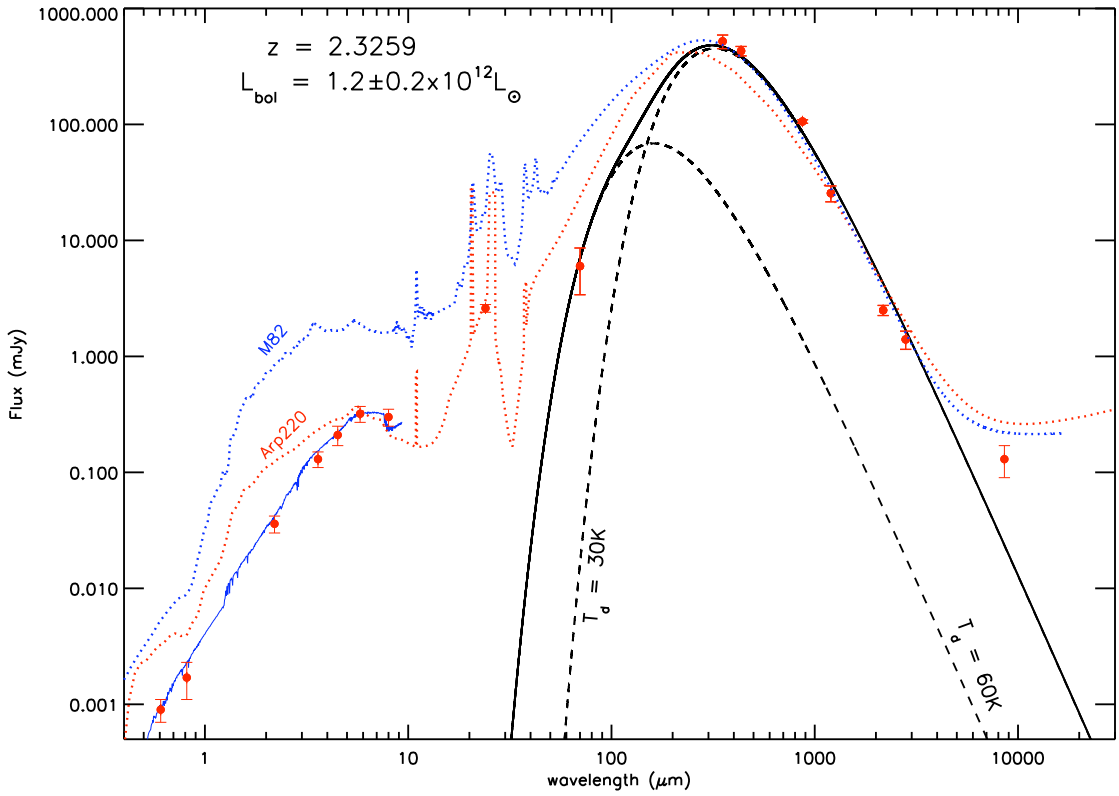

Figure 3 Spectral energy distribution of the galaxy lensed galaxy. To illustrate how the spectral energy distribution of the galaxy compares to local starbursts, we overlaid the spectral energy distributions from M82 (blue dashed line) and Arp220 (red dashed line), both scaled to equal flux at 1.2 mm. The solid black line denotes the best-fit spectrum, a two-component dust model with temperatures fixed at $T_{\rm d} = 30$ K and 60 K and a dust emissivity of $\beta = 1.8$ in a modified black-body function. We also overlaid the best-fit stellar spectral energy distribution to the optical to mid-infrared photometry (solid blue line) from which we estimate stellar age, extinction, luminosity and

Publisher: NPG; Journal: Nature: Nature; Article Type: Physics letter
DOI: 10.1038/nature08880

mass through population synthesis. The vertical error bars denote root-mean-square uncertainties in the measurements at each wavelength.

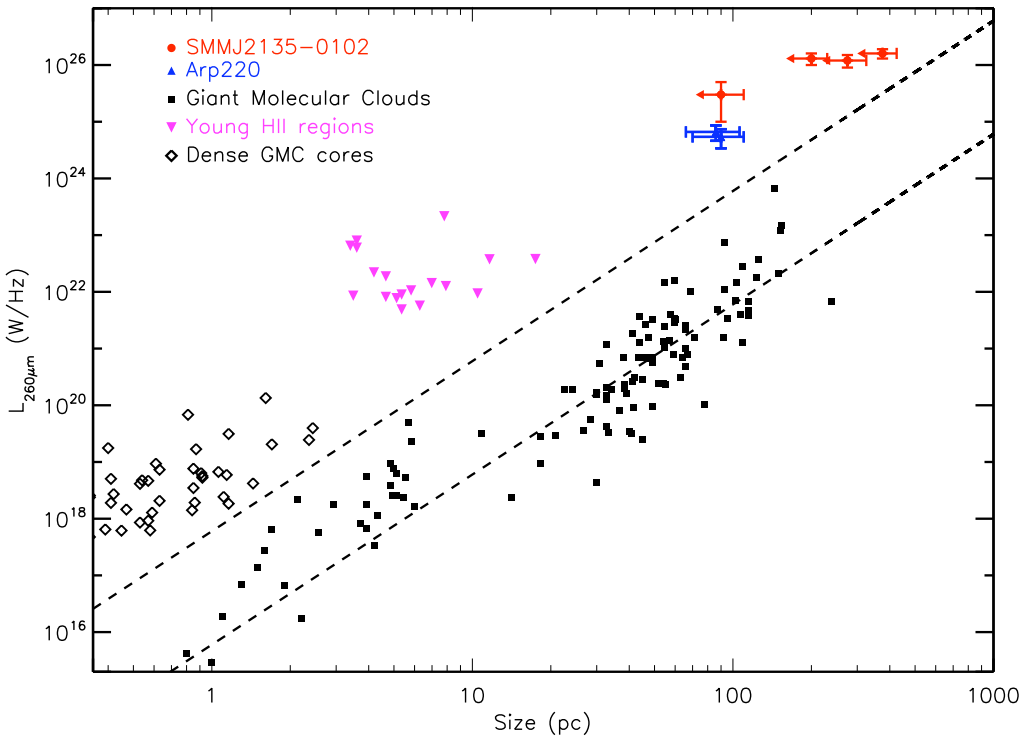

Figure 4 Relation between size and luminosity of star forming regions. Given that the star-forming regions in SMMJ2135−0102 are similar in size to giant molecular clouds in the Milky Way and local group galaxies, it is instructive to see how the luminosities compare with typical star-forming regions, as well as the dense star-forming cores inside many giant molecular clouds. Black squares denote the size and 260-μm luminosities of giant molecular clouds in the Milky Way and the Local Group[19,21–23], scaled from IRAS. In these comparison samples, we correct the rest-frame 100-μm luminosities to 260 μm by fitting a modified black-body to the 100-μm luminosity at the known temperature (which is derived from $L_{60\ \mu m}/L_{100\ \mu m}$ in each case). Because the peak of a 30-K black-body spectrum lies at ~170 μm, the correction is typically small, with a median $L_{260\ \mu m}/L_{100\ \mu m} = 1.5 \pm 0.4$. The lower dashed line shows the $L_{260} \propto r^3$ relation for constant energy density, a line with slope = 3. The solid red points denote the sizes and luminosities of the star-forming regions in SMMJ2135−0102 (the vertical errors denote the source-plane root-mean-square,

Publisher: NPG; Journal: Nature: Nature; Article Type: Physics letter
DOI: 10.1038/nature08880

while the horizontal errors denote the error in the source-plane FWHM measured from the range of acceptable lens models). The luminosities of the star-forming regions within SMMJ2135−0102 are about 100 times more luminous at a fixed size compared to local giant molecular clouds, so the upper dashed line shows the local fit but offset by a factor of a 100 in luminosity. We also plot the sizes and luminosities of dense cores of galactic giant molecular clouds[24] (open black diamonds), young (<3 Myr) H II regions in Henize 2-10 and M82 (inverted purple triangles), and the two dominant star-forming regions within the local ultra-luminous infrared galaxy Arp220[27] (blue triangles). In these comparison samples, the conversion between sub-millimetre flux and rest-frame 260-μm luminosity is also calculated using a modified black-body fit at known temperature (Supplementary Information).